Magnetic Circular Dichroism of the CH Radical in an Argon Matrix

Vaughan S. Langford and Bryce E. Williamson*

Department of Chemistry, University of Canterbury, Private Bag 4800, Christchurch, New Zealand

Received: September 4, 1997; In Final Form: October 24, 1997[⊗]

Magnetic circular dichroism (MCD) and absorption spectra are reported for the CH (methylidyne or methyne) free radical isolated in an Ar matrix (CH/Ar) over the temperature range 1.4−15.9 K and the magnetic-field range 0−4 T. Data for the A $^2\Delta \leftarrow$ X $^2\Pi$, B $^2\Sigma^- \leftarrow$ X $^2\Pi$, and C $^2\Sigma^+ \leftarrow$ X $^2\Pi$ band systems indicate a substantial quenching of the orbital angular momentum of the CH ground-state term. This is interpreted as being a consequence of crystal-field interactions involving atoms of the host lattice. Analysis of the zeroth moments of the spectra yields an empirical spin−orbit coupling constant $A_\Pi = 21 \pm 1$ cm^{-1} and orbital reduction factor $\kappa = 0.26 \pm 0.03$, corresponding to a crystal-field splitting of $V_\Pi = 78 \pm 14$ cm^{-1} for the X $^2\Pi$ term. For the A $^2\Delta$ excited-state term, the first MCD moments give $A_\Delta = 5 \pm 1$ cm^{-1}, and an upper limit of $V_\Delta \lesssim 15$ cm^{-1} is estimated from the dispersion of the MCD.

I. Introduction

This paper is the second in a series reporting the magnetic circular dichroism (MCD) and absorption spectra of free-radical monohydrides of the first-row elements isolated in Ar matrices (XH/Ar). In the first of the series we reported the spectra of OH/Ar[1] and provided a spin−orbit and crystal-field (SO−CF) model that explained the observed reduction of orbital angular momentum in terms of guest−host interactions. In this paper, we report temperature- and magnetic-field-dependent spectra for the CH (methylidyne or methyne) radical trapped in Ar (CH/Ar) and show that they can be interpreted within a similar theoretical framework.

The spectra of gas-phase CH are well understood[2,3] and have allowed the identification of the free radical in organic flames[4] and in a variety of extraterrestrial environments, including the interstellar medium,[5] cometary outflows,[6] and stars.[7,8] In contrast, there is a relative dearth of information concerning CH in condensed phases, such as rare-gas matrices. The first to conduct such studies were Robinson and McCarty,[9] who reported absorption spectra for the A $^2\Delta$, B $^2\Sigma^-$, and C $^2\Sigma^+ \leftarrow$ X $^2\Pi$ transitions of CH/Ar and CD/Ar formed by UV photolysis of diazomethane or its deuteriated analogues. Since then, Keyser has measured the absorption and emission spectra of the A $^2\Delta$, B $^2\Sigma^-$, and C $^2\Sigma^+$ systems of CH/Ar,[10] while Milligan and Jacox have reported the vibrational IR spectrum of both isotopomers.[11]

There has been only one prior study of the MCD of CH/Ar, conducted by Rose,[12] and limited to the A $^2\Delta \leftarrow$ X $^2\Pi$ and B $^2\Sigma^- \leftarrow$ X $^2\Pi$ transitions. She concluded from the MCD temperature dependence that the orbital angular momentum of the CH ground-state term is totally quenched in Ar.

In this paper, MCD and absorption spectra are reported for the A $^2\Delta \leftarrow$ X $^2\Pi$, B $^2\Sigma^- \leftarrow$ X $^2\Pi$, and C $^2\Sigma^+ \leftarrow$ X $^2\Pi$ transitions of CH/Ar at temperatures between 1.4 and 15.9 K and at magnetic fields up to 4 T. The results are interpreted in terms of a partial quenching of the ground-state orbital angular momentum, which is quantified by moment analysis within the framework of a SO−CF model. The A $^2\Delta$ excited-state term is also found to be subject to SO and CF effects involving interactions with Ar atoms of the host medium.

II. Experimental Section

MCD (ΔA) and double-beam absorption (A) spectra were measured simultaneously using a spectrometer described previously.[1,13] ΔA is the difference between the absorbance of left (A_+) and right (A_-) circularly polarized light by a sample in the presence of a longitudinal magnetic field (with inductance B), while A is the corresponding average;[14]

$$\Delta A = A_+ - A_- \quad (1)$$

$$A = (A_+ + A_-)/2 \quad (2)$$

Preliminary experiments were conducted using a closed-cycle He refrigerator (APD Cryogenics) and electromagnet[1,13] in order to determine optimum deposition and annealing conditions. All data reported below were obtained in later runs using an Oxford Instruments SM4 cryo-magnet and matrix injection system,[1,15,16] which permits more accurate and precise control of the magnetic field and sample temperature.

Matrices were prepared from ultrahigh-purity methane and Ar, mixed in a 1:100 mole ratio to a final pressure of ∼1 atm. The mixture was allowed to flow through a 9 mm (i.d.) quartz tube at a rate of ∼5 mmol h^{-1}, while being subjected to Ar-resonance radiation produced by a Tesla-coil discharge. The products were deposited onto a cryogenically cooled *c*-cut sapphire sample window held at ∼15 K. Deposition times were ∼15 min. Annealing resulted in slightly sharper bands, but did not significantly change the structure in the spectra and had the detrimental effects of reducing the CH concentration and clouding the matrices. For the data reported below, the matrices were not annealed.

Spectra of the A $^2\Delta$ and C $^2\Sigma^+$ systems were obtained using a spectral resolution of 0.08 nm (4.5 and 8 cm^{-1} respectively), while those of the B $^2\Sigma^-$ transition were acquired at a resolution of 0.16 nm (10 cm^{-1}).

* Corresponding author. E-mail: B.Williamson@chem.canterbury.ac.nz. Fax: ++ 64 3 364 2110.

[⊗] Abstract published in *Advance ACS Abstracts,* December 1, 1997.

S1089-5639(97)02882-X CCC: $15.00
Published on Web 01/01/1998

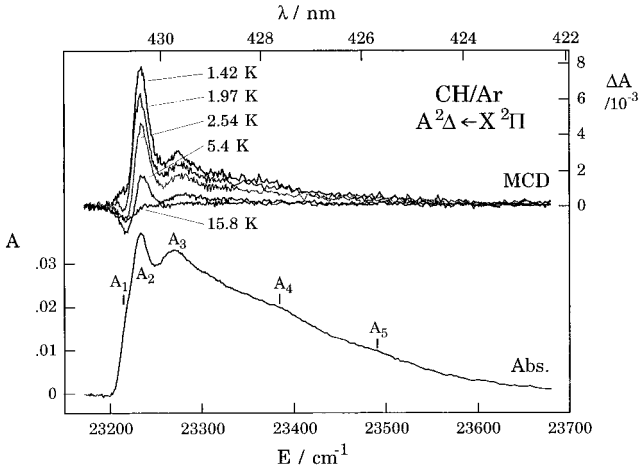

Figure 1. Absorption spectrum (bottom) and temperature dependence of the MCD (top; $B = 1$ T) for the A $^2\Delta \leftarrow$ X $^2\Pi$ transition of CH/Ar. Absorption bands are labeled for cross referencing with Table 1.

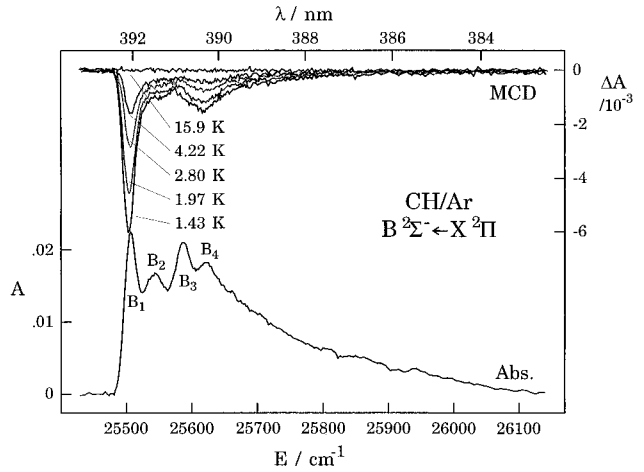

Figure 2. Absorption spectrum (bottom) and temperature dependence of the MCD (top; $B = 1$ T) for the B $^2\Sigma^- \leftarrow$ X $^2\Pi$ transition of CH/Ar. Absorption bands are labeled for cross referencing with Table 1.

III. Results

Absorption spectra and the temperature dependence of the MCD ($B = 1$ T) for the A $^2\Delta$, B $^2\Sigma^-$, and C $^2\Sigma^+$ systems of CH/Ar are presented in Figures 1−3. Representative MCD magnetic-field dependence data are shown in Figures 4−6.

In the matrix injection experiments a problem was encountered with OH contamination, which resulted in partial overlap of the C $^2\Sigma^+ \leftarrow$ X $^2\Pi$ transition of CH/Ar with the A $^2\Sigma^+ \leftarrow$ X $^2\Pi$ transition of OH/Ar. In an attempt to recover useful information from these spectra, the contributions from the OH impurity were digitally removed using comparisons with earlier data for OH/Ar spectra[1] and CH/Ar data obtained using the He-refrigerator/electromagnet system (which were free from significant contamination). Consequently, the data to the blue of ~314 nm in Figures 3 and 6 have been replaced by smooth curves, and analysis of the C $^2\Sigma^+ \leftarrow$ X $^2\Pi$ transition is subject to a greater level of uncertainty than those for the other transitions.

The absorption spectra are similar to, but of much higher quality (especially with regard to signal-to-noise ratio) than, those reported by Keyser[10] and Rose.[12] The positions of the individual bands are summarized in Table 1, where they are compared with previously reported values.[10,12] Each band system comprises a relatively sharp origin (A_2, B_1, and C_2 of Table 1) and a tail of broader bands to the blue, which have been assigned to overtones in librational and/or local-phonon modes.[10,12,13] Both the A $^2\Delta$ and C $^2\Sigma^+$ systems also show weak shoulders (A_1 and C_1, respectively) slightly to the red of the main origin bands, which are probably due to minor amounts of a secondary site.[12] The absorption spectra are only weakly temperature dependent, with the origin bands becoming slightly broader as the temperature is increased.

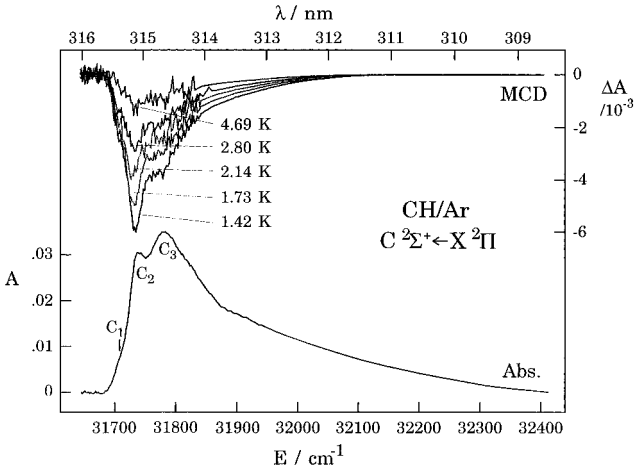

Figure 3. Absorption spectrum (bottom) and temperature dependence of the MCD (top; $B = 1$ T) for the C $^2\Sigma^+ \leftarrow$ X $^2\Pi$ transition of CH/Ar. Absorption bands are labeled for cross referencing with Table 1. Spectra have been corrected to compensate for OH contamination (see text).

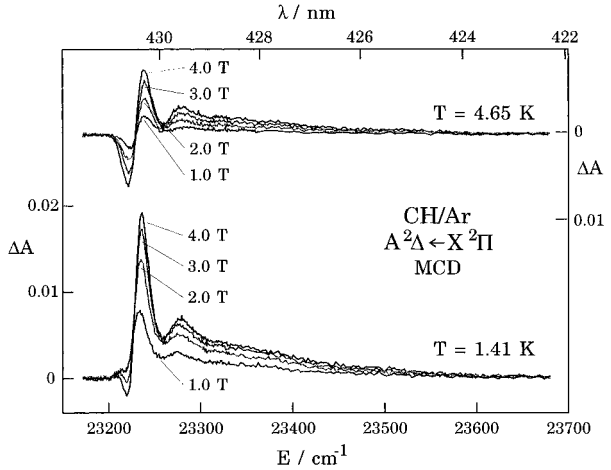

Figure 4. MCD magnetic-field dependence ($B = 1-4$ T) for the A $^2\Delta \leftarrow$ X $^2\Pi$ transition of CH/Ar.

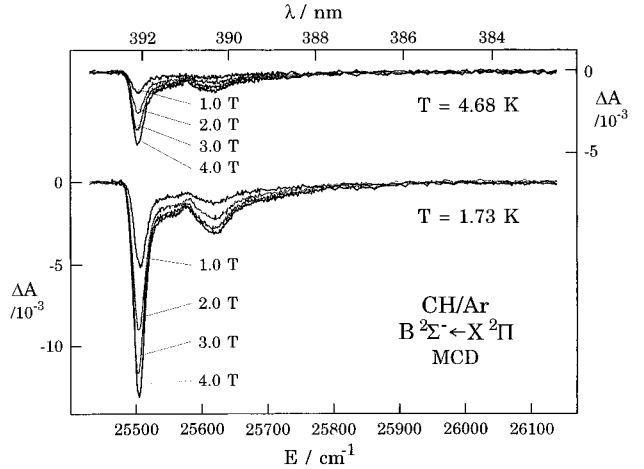

Figure 5. MCD magnetic-field dependence ($B = 1-4$ T) for the B $^2\Sigma^- \leftarrow$ X $^2\Pi$ transition of CH/Ar.

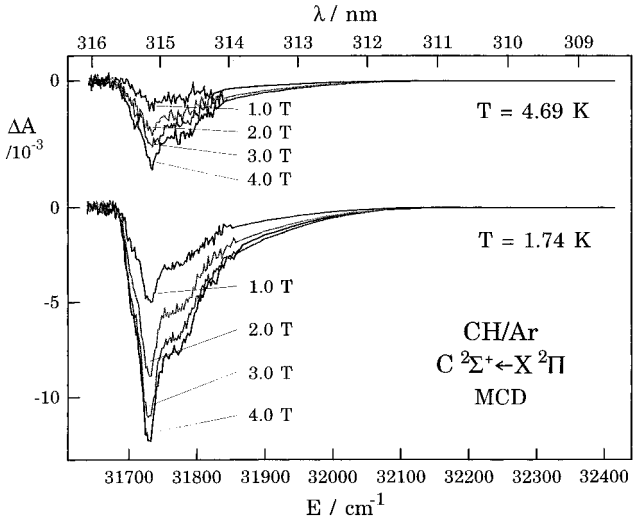

Figure 6. MCD magnetic-field dependence ($B = 1-4$ T) for the C $^2\Sigma^+ \leftarrow$ X $^2\Pi$ transition of CH/Ar. Data have been corrected for OH/Ar contamination (see text).

TABLE 1: Bands in the A $^2\Delta$, B $^2\Sigma^-$, and C $^2\Sigma^+ \leftarrow$ X $^2\Pi$ Systems of CH/Ar

	band energy/cm^{-1}		
band[a]	Keyser[10]	Rose[12]	this work[b]
A $^2\Delta \leftarrow$ X $^2\Pi$			
A_1		23 183	23 215 (−19)
A_2	23 170[c]	23 200	23 234 (0)
A_3	23 217	23 243	23 271 (37)
A_4			∼23 388 (154)
A_5			∼23 501 (267)
B $^2\Sigma^- \leftarrow$ X $^2\Pi$			
B_1	25 496	25 485	25 507 (0)
B_2		25 510	25 544 (37)
B_3	25 572	25 549	25 587 (80)
B_4		25 585[c]	25 622 (115)
C $^2\Sigma^+ \leftarrow$ X $^2\Pi$			
C_1	31 670		31 706 (−33)
C_2	31 710		31 739 (0)
C_3	31 738		31 780 (41)

[a] Band labeling is for cross reference with Figures 1−3. [b] Values in parentheses indicate shifts (in cm^{-1}) from the principal origin band. [c] Interpolated from figures in the relevant references.

The MCD spectra of the A $^2\Delta$ and B $^2\Sigma^-$ systems are in accord with those reported by Rose,[12] while the spectrum for the C $^2\Sigma^+ \leftarrow$ X $^2\Pi$ transition has not been reported previously. The MCD of the B $^2\Sigma^-$ and C $^2\Sigma^+$ systems is single signed and negative at all of the investigated temperatures. In contrast, that for the A $^2\Delta$ system is positive at low temperatures and becomes two-signed at higher temperatures. All of the transitions exhibit MCD with a reciprocal temperature dependence (Figures 1−3) and nonlinear magnetic-field dependence (Figures 4−6) characteristic of *C* terms.[14] To quantify these behaviors, dimensionless zeroth moments, $\mathbf{M}_0$ and $\mathbf{A}_0$ for MCD and absorption, respectively, are defined;

$$\mathbf{A}_0 = \int \frac{A(E)}{E}\,\mathrm{d}E \tag{3}$$

$$\mathbf{M}_0 = \int \frac{\Delta A(E)}{E}\,\mathrm{d}E \tag{4}$$

where E is the photon energy.

Figures 7 shows that (for $B = 1$ T) the dependence of $\mathbf{M}_0/\mathbf{A}_0$ on $1/kT$ ($k = 0.695$ cm^{-1} K^{-1} is Boltzmann's constant) is

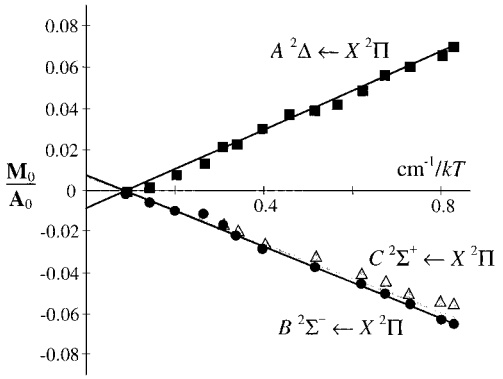

Figure 7. Temperature dependence of the moment ratio $\mathbf{M}_0/\mathbf{A}_0$ as a function of $1/kT$ for CH/Ar A $^2\Delta$, B $^2\Sigma^-$, and C $^2\Sigma^+ \leftarrow$ X $^2\Pi$ ($B = 1$ T). Lines are fits to the data obtained using eq 35 with the parameters in Table 4.

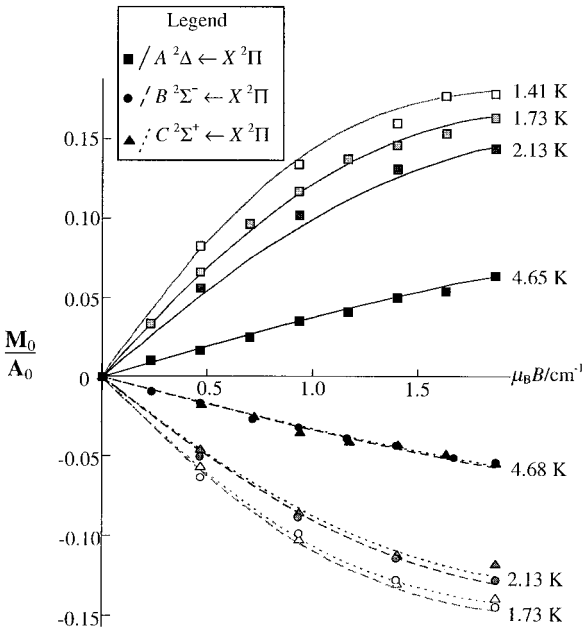

Figure 8. Field dependence of the moment ratio $\mathbf{M}_0/\mathbf{A}_0$ as a function of $\mu_B B$ for CH/Ar A $^2\Delta$, B $^2\Sigma^-$, and C $^2\Sigma^+ \leftarrow$ X $^2\Pi$. The curves are best fits to the data obtained using eqs 33 and 34 with the parameters in Table 4.

essentially linear for all three band systems. This type of behavior is a characteristic of MCD *C* terms in the so-called linear limit,[14] where $\mu_B B << kT$ ($\mu_B = 0.467$ cm^{-1} T^{-1} is the Bohr magneton). In addition, the ordinate intercepts are nonzero, which indicates the presence of *B* terms. Notably, in each case the intercept is of the opposite sign to the slope, with $\mathbf{M}_0/\mathbf{A}_0$ passing through zero at a temperature of ∼16 K. In Figure 8, plots are given for the same moment ratio against $\mu_B B$, at various temperatures between 4.7 and 1.4 K. At the higher temperatures, the plots deviate only slightly from linearity, but at lower temperatures the deviations are more marked, with $\mathbf{M}_0/\mathbf{A}_0$ tending toward an asymptotic limit at high values of $\mu_B B$. The latter effect is referred to as magnetization saturation and is also characteristic of *C* terms.[14]

It is clear from Figures 1−8 that MCD spectra of the B $^2\Sigma^-$ and C $^2\Sigma^+$ systems are qualitatively similar, with regard to their dispersions, negative signs, and temperature and field dependencies. On the other hand, the A $^2\Delta$ system has MCD of the opposite sign and at higher temperatures or magnetic fields shows a two-signed MCD, which is normally associated with *A* terms.[14]

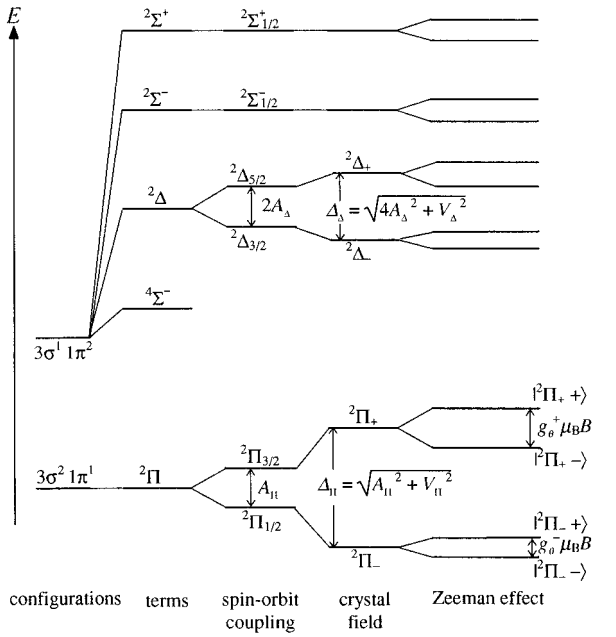

Figure 9. Energy-level diagram for CH/Ar (not to scale), showing the effects of spin−orbit, crystal-field, and Zeeman interactions on the X $^2\Pi$, A $^2\Delta$, B $^2\Sigma^-$, and C $^2\Sigma^+$ terms.

IV. Discussion

The A $^2\Delta$, B $^2\Sigma^-$ and C $^2\Sigma^+ \leftarrow$ X $^2\Pi$ transitions of CH formally arise from the excitation $3\sigma^1 1\pi^2 \leftarrow 3\sigma^2 1\pi^1$. The X $^2\Pi$ ground-state term is split by first-order spin−orbit (SO) interactions (Figure 9) into levels quantized by Ω, the projection of the total electronic angular momentum along the internuclear (z) axis. The SO states are designated $|^2\Pi_\Omega\ M_\Omega\rangle$, where $\Omega = 1/2$, 3/2 and $M_\Omega = \pm\Omega$. The corresponding SO energies are

$$E_{SO}(^2\Pi_\Omega) = A_\Pi \Lambda(\Omega - \Lambda) \tag{5}$$

where Λ (=1 for a Π state) is the projection of the orbital angular momentum along the internuclear (z) axis, and A_Π (=31.8 cm^{-1} in the gas phase[17]) is an empirical SO coupling constant for the X $^2\Pi$ term. The A $^2\Delta$, B $^2\Sigma^-$, and C $^2\Sigma^+$ terms do not exhibit first-order SO splitting, although the A $^2\Delta$ term is susceptible to higher order effects (vide infra).

C-term behavior in the MCD indicates the presence of states within the ground-state manifold that are both degenerate and susceptible to Zeeman splitting. (*C* terms result from differences between the thermal populations of Zeeman states.[14]) On this basis, any prospect of explaining the MCD of CH/Ar purely in terms of Zeeman perturbations of the SO states can be rejected, as follows. First, the $^2\Pi_{1/2}$ level shows no Zeeman splitting (within the limit $g_e \approx 2$), because the spin and orbital contributions to the magnetic moment cancel; consequently, *C* terms cannot be associated with transitions originating from the lower SO level. Second, although transitions from the $^2\Pi_{3/2}$ level give *C* terms, they are of the *opposite* sign to those observed in Figures 1−6.[13] And third, at the temperatures at which these experiments were conducted, the Boltzmann population of the $^2\Pi_{3/2}$ level would suggest weak *C* terms whose magnitude *decreases* as the temperature in decreased.

Incorporation of the radical into a matrix can lead to modifications of the SO states due to crystal-field (CF) interactions with the host atoms. It has been demonstrated previously, for TiO/Ar[18] and OH/Ar,[1] that such modifications can profoundly effect the MCD, principally through partial quenching of the orbital angular momentum. The treatment that follows for CH/Ar is similar to that presented previously for OH/Ar,[1] but with some significant differences. First, the X $^2\Pi$ term of CH is a regular SO system, whereas the equivalent for OH is inverted. Second, the magnitude of the ground-state SO coupling is substantially weaker in CH. Third, for CH/Ar there are three (rather than one) transitions to be considered. And fourth, the orbitally degenerate A $^2\Delta$ excited-state term is also susceptible to SO and CF effects.

The orbitally degenerate X $^2\Pi$ and A $^2\Delta$ terms are susceptible to CF splittings, which in the following are denoted V_Π and V_Δ, respectively. In each case, the active CF component must transform as part of the symmetric square of the orbital irrep. Hence, V_Π and V_Δ arise from CFs of different symmetry ($[\Pi^2] \supset \Delta$ and $[\Delta^2] \supset \Gamma$), and their magnitudes may be quite different. Since $\mathbf{M}_0$ and $\mathbf{A}_0$ are invariant to unitary transformations of the excited-state bases (and therefore independent of excited-state CF splittings), discussion initially centers on the X $^2\Pi$ term. The overall SO−CF splitting for this term (Figure 9), obtained by solution of the appropriate 2×2 secular equation, is

$$\Delta_\Pi = (A_\Pi^2 + V_\Pi^2)^{1/2} \tag{6}$$

The corresponding eigenfunctions are

$$|^2\Pi_+ \pm 1/2\rangle = \mp\beta|^2\Pi_{1/2} \mp 1/2\rangle + \alpha|^2\Pi_{3/2} \pm 3/2\rangle \tag{7}$$

$$|^2\Pi_- \pm 1/2\rangle = \alpha|^2\Pi_{1/2} \mp 1/2\rangle \pm \beta|^2\Pi_{3/2} \pm 3/2\rangle \tag{8}$$

where, in the left-hand sets, $^2\Pi_+$ and $^2\Pi_-$ designate the upper and lower SO−CF levels, respectively, and $\pm 1/2$ denotes the value of the spin quantum number, M_S. The mixing coefficients α and β, and relationships between them, are

$$\alpha = V_\Pi/(V_\Pi^2 + (\Delta_\Pi - A_\Pi)^2)^{1/2} \tag{9}$$

$$\beta = (\Delta_\Pi - A_\Pi)/(V_\Pi^2 + (\Delta_\Pi - A_\Pi)^2)^{1/2} \tag{10}$$

$$\alpha^2 + \beta^2 = 1 \tag{11}$$

$$\alpha^2 - \beta^2 = A_\Pi/\Delta_\Pi \equiv \kappa \tag{12}$$

$$2\alpha\beta = V_\Pi/\Delta_\Pi \equiv \eta \tag{13}$$

The CF acts to redistribute the orbital angular momentum of the SO states. The relevant matrix elements for a $^2\Pi$ term are listed in Table 2 of ref 1, but the g values are now

$$g_{||}^{\pm} \equiv 2\langle^2\Pi_\pm +1/2|L_z + g_e S_z|^2\Pi_\pm +1/2\rangle = g_e \pm 2\kappa \tag{14}$$

$$g_\perp \equiv 2\langle^2\Pi_\pm +1/2|L_x + g_e S_x|^2\Pi_\pm -1/2\rangle = g_e\eta \tag{15}$$

where the components of the angular momentum operators **L** and **S** refer to the molecular (x, y, z) reference frame. κ is the orbital reduction factor and can take values between 1 ($V_\Pi = 0$) and 0 ($V_\Pi >> A_\Pi$). Note that because the X $^2\Pi$ term of CH is regular, the sign of the κ term in eq 14 is opposite to that for OH/Ar,[1] and the equations for the $g_{||}^{\pm}$ values are reversed. Consequently, $g_{||}^{-} = 0$ when $\kappa = 1$ and *increases* toward the spin-only value as κ decreases to zero.

Expressions can now be derived for the MCD and absorbance associated with transitions originating from the X $^2\Pi$ states. We start by considering the zeroth moments $\mathbf{A}_0$ and $\mathbf{M}_0$ defined

by eqs 3 and 4. In the conventional theoretical formalism for MCD, $\mathbf{M}_0$ contains contributions from B and C terms;[14]

$$\mathbf{M}_0 = \mathbf{B}_0 + \mathbf{C}_0 \tag{16}$$

$\mathbf{C}_0$ is a function of the populations of the states from which the transitions originate and is therefore dependent on the Zeeman shifts of these states. $\mathbf{B}_0$ is a consequence of magnetic-field-induced mixing of states and does not depend directly on the Zeeman shifts. In the following, $\mathbf{C}_0$ is considered first, along with $\mathbf{A}_0$. $\mathbf{B}_0$ is then treated by application of nondegenerate perturbation theory. Expressions are initially derived for molecules with a fixed, arbitrary orientation and then extended appropriately for the case of a randomly oriented ensemble.

For OH/Ar, theoretical expressions for the MCD were derived assuming that only the lowest SO−CF level carries a significant Boltzmann population.[1] However, for CH/Ar, the gas-phase SO splitting is substantially smaller and could be further reduced by matrix effects. It is therefore prudent to consider, at least initially, that the upper level may be populated. (In fact, as will be shown later, the $^2\Pi_+$ level is not significantly populated at the temperatures used in these experiments, since any reduction in the SO splitting is more than compensated for by a larger CF splitting.)

Consider a molecule whose internuclear axis is oriented at angle θ with respect to the magnetic field direction. For the X $^2\Pi$ SO−CF levels, the first-order Zeeman states and corresponding shifts are

$$|^2\Pi_\sigma\pm\rangle = a_\sigma|^2\Pi_\sigma \pm 1/2\rangle \pm b_\sigma|^2\Pi_\sigma \mp 1/2\rangle \tag{17}$$

$$E_B(^2\Pi_\sigma\pm) = \pm g_\theta^\sigma \mu_B B/2 \tag{18}$$

where $\sigma = \pm$ labels the SO−CF level and the '+' and '−' on the left-hand side indicate the raised and lowered Zeeman states, respectively. The coefficients a_σ and b_σ satisfy the relations

$$|a_\sigma|^2 = (g_\perp \sin\theta)^2/(2g_\theta^\sigma(g_\theta^\sigma - g_{||}{}^\sigma \cos\theta)) \tag{19}$$

$$|a_\sigma|^2 + |b_\sigma|^2 = 1 \tag{20}$$

$$|a_\sigma|^2 - |b_\sigma|^2 = g_{||}{}^\sigma \cos\theta/g_\theta^\sigma \tag{21}$$

where $g_{||}{}^\sigma$ is given by eq 14, and

$$g_\theta^\sigma = ((g_{||}{}^\sigma \cos\theta)^2 + (g_\perp \sin\theta)^2)^{1/2} \tag{22}$$

The net SO−CF splitting is Δ_Π, so the fractional Boltzmann populations are

$$P_-(\pm) = \frac{1}{Q}\exp\left(\mp\frac{g_\theta^- \mu_B B}{2kT}\right)\exp(\Delta_\Pi/2kT) \tag{23}$$

$$P_+(\pm) = \frac{1}{Q}\exp\left(\mp\frac{g_\theta^+ \mu_B B}{2kT}\right)\exp(-\Delta_\Pi/2kT) \tag{24}$$

where Q is the partition function.

After transforming to a molecule-fixed reference frame (eqs 24 and 25 of ref 1), the contributions to $\mathbf{A}_0$ and $\mathbf{C}_0$ from a component transition to excited state λ within the J manifold are

$$\mathbf{A}_0^\theta(J\lambda\leftarrow{}^2\Pi_\sigma\pm) = \frac{\gamma(1+\cos^2\theta)}{4}\sum_\lambda P_\sigma(\pm)(|\langle J\lambda|m_{+1}|^2\Pi_\sigma\pm\rangle|^2 + |\langle J\lambda|m_{-1}|^2\Pi_\sigma\pm\rangle|^2) \tag{25}$$

$$\mathbf{C}_0^\theta(J\lambda\leftarrow{}^2\Pi_\sigma\pm) = \gamma\cos\theta\sum_\lambda P_\sigma(\pm)(|\langle J\lambda|m_{+1}|^2\Pi_\sigma\pm\rangle|^2 - |\langle J\lambda|m_{-1}|^2\Pi_\sigma\pm\rangle|^2) \tag{26}$$

where common factors, including refractive index corrections and the concentration and path length of the sample, are collected in the coefficient γ.

$\mathbf{A}_0$ and $\mathbf{M}_0$ are invariant to unitary transformations of the excited-state bases[14] (as long as the integrals in eqs 3 and 4 are carried over all component transitions); hence there is flexibility in the choice of the $|J\lambda\rangle$ of eqs 25 and 26. In fact it is most efficient to use SO basis states, ignoring (for the moment) the possibility of CF effects in the A $^2\Delta$ term. If all transitions are taken to arise from the $3\sigma^1 1\pi^2 \leftarrow 3\sigma^2 1\pi^1$ excitation, the corresponding transition moments can be related to one another; the results are summarized in Table 2, where M is the reduced one-electron transition moment for the excitation $1\pi \leftarrow 3\sigma$,

$$M = \langle 1\pi||m||3\sigma\rangle \tag{27}$$

Using these integrals and summing over all component transitions, $\mathbf{A}_0$ and $\mathbf{C}_0$ for the different band systems are found to be related by factors $Z_A(J)$ and $Z_M(J)$, respectively, which are given in Table 3. The results are

$$\mathbf{A}_0^\theta(J\leftarrow{}^2\Pi) = \frac{Z_A(J)\,\gamma(1+\cos^2\theta)|M|^2}{8} \tag{28}$$

$$\mathbf{C}_0^\theta(J\leftarrow{}^2\Pi) = \frac{Z_M(J)\gamma\kappa\cos^2\theta|M|^2}{Q}\left[\frac{g_{||}{}^-}{g_\theta{}^-}\sinh\left(\frac{g_\theta{}^-\mu_B B}{2kT}\right)\times\exp(\Delta_\Pi/2kT) - \frac{g_{||}{}^+}{g_\theta{}^+}\sinh\left(\frac{g_\theta{}^+\mu_B B}{2kT}\right)\exp(-\Delta_\Pi/2kT)\right] \tag{29}$$

In eq 29, the first and second terms in the square brackets give the C-term contributions of transitions originating from the lower ($^2\Pi_-$) and upper ($^2\Pi_+$) SO−CF levels, respectively. Note that a finite $\mathbf{C}_0$ requires $\kappa > 0$, so the experimental observation of a temperature-dependent $\mathbf{M}_0$ certifies that the ground-state orbital angular momentum of CH is not completely quenched by the Ar matrix.

B-term contributions to the MCD are now determined by considering magnetic-field-induced mixing of the SO−CF states within the X $^2\Pi$ manifold. Following standard first-order nondegenerate perturbation theory, and transforming to the molecular reference frame, the corrections to the wave functions

TABLE 2: Transition Moments for the A $^2\Delta$, B $^2\Sigma^-$, C $^2\Sigma^+$ ← X $^2\Pi_\pm$ Transitions of CH/Ar[a]

m_{+1}	$\|^2\Pi_- -\rangle$	$\|^2\Pi_- +\rangle$	$\|^2\Pi_+ -\rangle$	$\|^2\Pi_+ +\rangle$
$\langle^2\Delta_{3/2}\ -3/2\|$	0	0	0	0
$\langle^2\Delta_{3/2}\ 3/2\|$	$-a_-\alpha M/\sqrt{2}$	$-b_-\alpha M/\sqrt{2}$	$-a_+\beta M/\sqrt{2}$	$-b_+\beta M/\sqrt{2}$
$\langle^2\Delta_{5/2}\ -5/2\|$	0	0	0	0
$\langle^2\Delta_{5/2}\ 5/2\|$	$-b_-\beta M/\sqrt{2}$	$a_-\beta M/\sqrt{2}$	$-b_+\alpha M/\sqrt{2}$	$a_+\alpha M/\sqrt{2}$
$\langle^2\Sigma^-_{1/2}\ -1/2\|$	$\sqrt{3}a_-\beta M/2$	$\sqrt{3}b_-\beta M/2$	$-\sqrt{3}a_+\alpha M/2$	$-\sqrt{3}b_+\alpha M/2$
$\langle^2\Sigma^-_{1/2}\ 1/2\|$	$\sqrt{3}b_-\alpha M/2$	$-\sqrt{3}a_-\alpha M/2$	$-\sqrt{3}b_+\beta M/2$	$\sqrt{3}a_+\beta M/2$
$\langle^2\Sigma^+_{1/2}\ -1/2\|$	$a_-\beta M/2$	$b_-\beta M/2$	$-a_+\alpha M/2$	$-b_+\alpha M/2$
$\langle^2\Sigma^+_{1/2}\ 1/2\|$	$-b_-\alpha M/2$	$a_-\alpha M/2$	$b_+\beta M/2$	$-a_+\beta M/2$
m_{-1}	$\|^2\Pi_- -\rangle$	$\|^2\Pi_- +\rangle$	$\|^2\Pi_+ -\rangle$	$\|^2\Pi_+ +\rangle$
$\langle^2\Delta_{3/2}\ -3/2\|$	$b_-\alpha M/\sqrt{2}$	$-a_-\alpha M/\sqrt{2}$	$-b_+\beta M/\sqrt{2}$	$a_+\beta M/\sqrt{2}$
$\langle^2\Delta_{3/2}\ 3/2\|$	0	0	0	0
$\langle^2\Delta_{5/2}\ -5/2\|$	$-a_-\beta M/\sqrt{2}$	$-b_-\beta M/\sqrt{2}$	$a_+\alpha M/\sqrt{2}$	$b_+\alpha M/\sqrt{2}$
$\langle^2\Delta_{5/2}\ 5/2\|$	0	0	0	0
$\langle^2\Sigma^-_{1/2}\ -1/2\|$	$\sqrt{3}a_-\alpha M/2$	$\sqrt{3}b_-\alpha M/2$	$\sqrt{3}a_+\beta M/2$	$\sqrt{3}b_+\beta M/2$
$\langle^2\Sigma^-_{1/2}\ 1/2\|$	$\sqrt{3}b_-\beta M/2$	$-\sqrt{3}a_-\beta M/2$	$-\sqrt{3}b_+\alpha M/2$	$-\sqrt{3}a_+\alpha M/2$
$\langle^2\Sigma^+_{1/2}\ -1/2\|$	$-a_-\alpha M/2$	$-b_-\alpha M/2$	$-a_+\beta M/2$	$-b_+\beta M/2$
$\langle^2\Sigma^+_{1/2}\ 1/2\|$	$b_-\beta M/2$	$-a_-\beta M/2$	$b_+\alpha M/2$	$-a_+\alpha M/2$

[a] M is defined in eq 27.

are

$$|^2\Pi_- \pm\rangle' = -\frac{\mu_B B}{2\Delta_\Pi}[(a_- g_\perp \cos\theta + 2b_-\,\kappa \sin\theta)|^2\Pi_+ \pm 1/2\rangle \pm (b_-\, g_\perp \cos\theta - 2a_-\,\kappa \sin\theta)|^2\Pi_+ \mp 1/2\rangle] \quad (30)$$

$$|^2\Pi_+ \pm\rangle' = +\frac{\mu_B B}{2\Delta_\Pi}[(a_+\, g_\perp \cos\theta - 2b_+\,\kappa \sin\theta)|^2\Pi_- \pm 1/2\rangle \pm (b_+\, g_\perp \cos\theta + 2a_+\,\kappa \sin\theta)|^2\Pi_- \mp 1/2\rangle] \quad (31)$$

The corresponding first-order corrections to the transition moments yield the B-term contributions to the MCD;

$$\mathbf{B}_0^\theta(J\leftarrow^2\Pi) = \frac{-Z_M(J)\,\gamma(g_\perp \cos\theta)^2\mu_B B|M|^2}{2Q\Delta_\Pi}\left[\cosh\left(\frac{g_\theta^-\mu_B B}{2kT}\right)\times \exp(\Delta_\Pi/2kT) - \cosh\left(\frac{g_\theta^+\mu_B B}{2kT}\right)\exp(-\Delta_\Pi/2kT)\right] \quad (32)$$

Again, the first and second terms in the square brackets pertain to transitions originating in the lower and upper SO−CF levels, respectively.

Equations 28, 29, and 32 are in qualitative accord with the experimental data. First, $\mathbf{A}_0$ should be temperature independent (eq 28), whereas $\mathbf{M}_0$ should exhibit (potentially complicated) temperature dependence (eqs 29 and 32). Second, at low temperatures, where C terms are dominant and the $^2\Pi_-$ level carries the greater population, the MCD signs will be determined by the coefficients $Z_M(J)$. More precisely, the first term within the square brackets of eq 29 will dominate, and since all parameters within that term are either squared or intrinsically positive, A $^2\Delta$ ← X $^2\Pi$ should be associated with positive MCD, while the other two transitions are associated with negative MCD. Finally, the leading negative sign in eq 32 indicates that the B terms are of opposite sign to the C terms; that is, the temperature-dependence plots in Figure 7 should change sign as the temperature is increased.

TABLE 3: Absorption and MCD Moment Coefficients for J ← X $^2\Pi$ Transitions of CH/Ar

excited term (J)	$Z_A(J)$	$Z_M(J)$	$Z(J) = Z_M(J)/Z_A(J)$
A $^2\Delta$	1.0	1.0	1
B $^2\Sigma^-$	1.5	−1.5	−1
C $^2\Sigma^+$	0.5	−0.5	−1

Despite the qualitative compatibility of theory and experiment, there is one significant quantitative inconsistency. The experimental $\mathbf{A}_0$ values are in the ratio A $^2\Delta$:B $^2\Sigma^-$:C $^2\Sigma^+$ = 1:0.68:∼1, which (given the problems with OH contamination in the vicinity of the C $^2\Sigma^+$ system) is in reasonable accord with gas-phase values (converted from oscillator strengths) of 1:0.69:1.7.[19] On the other hand, the predicted ratios, assuming a common ($1\pi \leftarrow 3\sigma$) excitation, are 1:1.5:0.5 (Table 3). This discrepancy may signify a substantial degree of excited-state configuration interaction. For the purposes the current work, the problem can be circumvented by taking the ratios of the MCD and absorption moments. The utility of this procedure ensues from the fact that the corresponding coefficient ratios, $Z(J) = Z_A(J)/Z_M(J)$ (Table 3), are determined entirely by the symmetries of the excited states and are independent of configurational parentage. Moreover, it confers the advantage of cancelling the factor γ. Taking the appropriate ratios, and at the same time averaging over θ, gives

$$\frac{\mathbf{C}_0(J\leftarrow^2\Pi)}{\mathbf{A}_0(J\leftarrow^2\Pi)} = 3\kappa Z(J)\left[g_{||}^-\exp(\Delta_\Pi/2kT)\int_0^1\frac{\cos^2\theta}{Qg_\theta^-}\times \sinh\left(\frac{g_\theta^-\mu_B B}{2kT}\right)\mathrm{d}\cos\theta - g_{||}^+\exp(-\Delta_\Pi/2kT)\int_0^1\frac{\cos^2\theta}{Qg_\theta^+}\times \sinh\left(\frac{g_\theta^+\mu_B B}{2kT}\right)\mathrm{d}\cos\theta\right] \quad (33)$$

$$\frac{\mathbf{B}_0(J\leftarrow^2\Pi)}{\mathbf{A}_0(J\leftarrow^2\Pi)} = -\frac{3\mu_B B Z(J)}{\Delta_\Pi}\left[\exp(\Delta_\Pi/2kT)\int_0^1\frac{(g_\perp\cos\theta)^2}{Q}\times \cosh\left(\frac{g_\theta^-\mu_B B}{2kT}\right)\mathrm{d}\cos\theta - \exp(-\Delta_\Pi/2kT)\int_0^1\frac{(g_\perp\cos\theta)^2}{Q}\times \cosh\left(\frac{g_\theta^+\mu_B B}{2kT}\right)\mathrm{d}\cos\theta\right] \quad (34)$$

The temperature and magnetic-field dependencies indicated by eqs 33 and 34 are potentially very complicated and are certainly not amenable to analytical solution. However, if $\Delta_\Pi >> kT$, only the $^2\Pi_-$ state will be significantly populated and the situation is substantially simplified. There are reasons for believing that this should be the case for CH/Ar at $T \lesssim 16$ K. With $\Delta_\Pi \approx 32$ cm^{-1} (the gas-phase value of A_Π), the fractional population of the $^2\Pi_+$ level would be less than 3%. Although external-atom effects tend to reduce the SO splittings of impurities in matrices,[20,21] Δ_Π is almost certainly increased by CF effects (eq 6). It is therefore likely that the population of the $^2\Pi_+$ level is negligible. Both the signs of the MCD (as discussed above) and the linearity of the plots in Figure 7 support this conclusion. The latter can be illustrated by dropping the $^2\Pi_+$ contributions from eqs 33 and 34 and then invoking the linear limit to allow analytical determination of the integrals

TABLE 4: Parameters for the X $^2\Pi$ Term of CH/Ar

system	A_Π/cm^{-1}	κ	V_Π/cm^{-1}	Δ_Π/cm^{-1}	$g_{\|\|}^-$	$g_\perp$
A $^2\Delta \leftarrow$ X $^2\Pi$	22	0.28	77	80	1.44	1.92
B $^2\Sigma^- \leftarrow$ X $^2\Pi$	21	0.24	85	88	1.52	1.94
C $^2\Sigma^+ \leftarrow$ X $^2\Pi$	21	0.23	89	91	1.54	1.95
overall	21 ± 1	0.26 ± 0.03	78 ± 14	81 ± 14	1.48 ± 0.07	1.93 ± 0.02

over θ. The result is

$$\frac{\mathbf{M}_0(J\leftarrow{}^2\Pi)}{\mathbf{A}_0(J\leftarrow{}^2\Pi)} \approx Z(J)\mu_B B\left[\frac{(1-\kappa)\kappa}{kT} - \frac{g_e{}^2(1-\kappa^2)}{2\Delta_\Pi}\right] \quad (\Delta_\Pi >> kT >> \mu_B B) \quad (35)$$

Equations 33−35 are functions of only two independent parameters, which were determined by least-squares fitting of the data in Figures 7 and 8. The procedure is similar to that used for OH/Ar,[1] except that weaker SO coupling precludes assumption of a value for A_Π. The free parameters were chosen to be κ and A_Π, initial estimates for which were obtained by using eq 35 and the data in Figure 7. Refined values were then obtained independently for each band system by fitting eqs 33 and 34 to the data in Figure 8. The population of the $^2\Pi_+$ level was assumed to be zero, and the integrals over θ were evaluated numerically. The best fits, illustrated by the curves in Figure 8, provide very credible representations of the experimental results. In particular, the temperature dependencies of the saturation curves are accurately reproduced both in terms of magnitude and degree of curvature.

Table 4 summarizes the final values obtained from the fits and some of the pertinent parameters derived from them. The values for A_Π are consistent across all three systems, but there is some variation in κ. The latter is reflected in the different absolute slopes of the data shown in Figure 7. In the case of the C $^2\Sigma^+$ system, errors were almost certainly introduced during the procedure to correct the spectra for OH contamination. The main reason for the discrepancy between the data for the other systems probably lies with systematic uncertainties in determining the absorption baselines at low optical densities. Combining the results for all three transitions gives a SO coupling constant of $A_\Pi = 21 \pm 1$ cm^{-1} (reduced by $\sim$11 cm^{-1} from the gas-phase value[17]) and an orbital reduction factor of $\kappa = 0.26 \pm 0.03$.

With eqs 6 and 12, the results in Table 4 give $V_\Pi \approx 78 \pm 14$ cm^{-1} and $\Delta_\Pi \approx 81 \pm 14$ cm^{-1}. The former is similar to the (average) value of 97 ± 10 cm^{-1} found for OH/Ar.[1] The latter allows a test of the assumption that the $^2\Pi_+$ level is not significantly populated at the temperatures ($T \lesssim 16$ K) investigated in this work. With an upper limit of $P_+(\pm) \lesssim 10^{-3}$, the assumption is definitely justified.

The discussion of the MCD has so far concerned only *B* and *C* terms and their contributions to the $\mathbf{M}_0$. At higher temperatures and stronger magnetic fields, the A $^2\Delta$ system shows two-signed MCD (Figures 1 and 4), which is normally associated with *A* terms. These have a sigmoidal band shape, are temperature independent, and occur when the initial and/or final states are split by the Zeeman effect.[14] In the case of a degenerate initial state, *A* terms become more apparent at higher temperatures, being overwhelmed by *C* terms at lower temperatures. All of the transitions of CH/Ar fit the criteria required to show *A* terms; the question therefore arises as to why they are discernible only in the case of the A $^2\Delta$ system.

The strength of an *A* term is quantified by the first moment, $\mathbf{M}_1$, of the MCD;

$$\mathbf{M}_1 = \int \frac{\Delta A(E)}{E}(E - \bar{E})\mathrm{d}E \quad (36)$$

$\bar{E}$ is the barycenter of the absorption, and the integral is carried over the complete envelope of the band system. The procedure for generating theoretical expressions for $\mathbf{M}_1$ is similar to that described above for $\mathbf{M}_0$. Since $\mathbf{M}_1$ is also independent of excited-state CF effects,[14] it is again convenient to use the SO excited-state basis functions. Taking the population of the $^2\Pi_+$ level to be zero, the results for the three-band systems of CH/Ar are

$$\mathbf{M}_1^\theta(\mathrm{A}^2\Delta\leftarrow{}^2\Pi) = \frac{\gamma|M|^2\cos^2\theta}{2}\left[(2-\kappa^2)\mu_B B - A_\Delta(1-\kappa^2)\tanh\left(\frac{g_\theta{}^-\mu_B B}{2kT}\right)\right] \quad (37)$$

$$\mathbf{M}_1^\theta(\mathrm{B}^2\Sigma^-\leftarrow{}^2\Pi) = 3\kappa^2\mu_B B\cos^2\theta|M|^2/4 \quad (38)$$

$$\mathbf{M}_1^\theta(\mathrm{C}^2\Sigma^+\leftarrow{}^2\Pi) = \kappa^2\mu_B B\cos^2\theta|M|^2/4 \quad (\Delta_\Pi >> kT) \quad (39)$$

All terms in eqs 37−39 represent conventional *A* terms, except for the second in the square brackets of eq 37, which is temperature dependent and arises from *C* terms that are shifted by excited-state SO effects; A_Δ is the empirical SO coupling parameter for the A $^2\Delta$ term (Figure 9). From Table 4, $\kappa^2 \approx 0.07$; accordingly, $\mathbf{M}_1$ for the B $^2\Sigma^-$ and C $^2\Sigma^+$ systems is strongly quenched by the CF of the matrix, which explains the single-signed nature of their MCD. On the other hand, $\mathbf{M}_1$ for the A $^2\Delta$ system is substantially enhanced, especially at higher temperatures, where the temperature-independent contributions to the MCD are dominant and $\mathbf{M}_1/\mathbf{M}_0 \approx \Delta_\Pi$. Hence the A $^2\Delta$ system shows a two-signed MCD at high temperatures (Figures 1 and 4).

After orientational averaging, invoking the linear limit, and dividing through by the appropriate $\mathbf{A}_0$, eqs 37−39 become

$$\frac{\mathbf{M}_1(\mathrm{A}^2\Delta\leftarrow\mathrm{X}^2\Pi)}{\mathbf{A}_0(\mathrm{A}^2\Delta\leftarrow\mathrm{X}^2\Pi)} = \mu_B B\left[(2-\kappa^2) + \left(\frac{A_\Delta(\kappa^2-1)g_{||}{}^-}{2kT}\right)\right] \quad (40)$$

$$\frac{\mathbf{M}_1(\mathrm{B}^2\Sigma^-\leftarrow\mathrm{X}^2\Pi)}{\mathbf{A}_0(\mathrm{B}^2\Sigma^-\leftarrow\mathrm{X}^2\Pi)} = \frac{\mathbf{M}_1(\mathrm{C}^2\Sigma^+\leftarrow\mathrm{X}^2\Pi)}{\mathbf{A}_0(\mathrm{C}^2\Sigma^+\leftarrow\mathrm{X}^2\Pi)} = \kappa^2\mu_B B \quad (\Delta_\Pi >> kT >> \mu_B B) \quad (41)$$

From eq 40, it can be seen that the temperature and magnetic-field dependencies of $\mathbf{M}_1/\mathbf{A}_0$ provide information about the SO splitting ($2A_\Delta$; Figure 9) of the A $^2\Delta$ term. With $\kappa = 0.26 \pm 0.03$, moment analysis of the magnetic-field-dependence data in Figure 4 yields $A_\Delta = 5 \pm 1$ cm^{-1}. That is (neglecting excited-state CF splitting, to which $\mathbf{M}_1$ is insensitive), the $^2\Delta_{5/2}$ level of CH/Ar lies $\sim$10 cm^{-1} above the $^2\Delta_{3/2}$ level. Analysis of the temperature dependence is less precise due to uncertainties of

determining $\mathbf{M}_1$ at low temperatures in the presence of a very much larger $\mathbf{M}_0$, but the data in Figure 1 give $A_\Delta = 6 \pm 2$ cm^{-1}. In contrast, $A_\Delta = -1.1 \pm 0.2$ cm^{-1} for CH in the gas phase,[17] which indicates that the matrix imposes a substantial external-atom SO effect on the A $^2\Delta$ states.

$\mathbf{M}_0$ and $\mathbf{M}_1$ yield no information about V_Δ, the CF splitting of the A $^2\Delta$ term. However, an upper-limit estimate can be obtained from the separation of ~18 cm^{-1} between the maximum and minimum of the strong A-term feature centered at ~23 230 cm^{-1}. Setting $\Delta_\Delta = (V_\Delta^2 + 4A_\Delta^2)^{1/2} \lesssim 18$ cm^{-1} gives $V_\Delta \lesssim 15$ cm^{-1}, which is substantially smaller than the CF splitting of the ground-state term.

V. Conclusion

Temperature- and magnetic-field-dependence studies of the MCD associated with the A $^2\Delta$, B $^2\Sigma^-$, and C $^2\Sigma^+ \leftarrow$ X $^2\Pi$ systems of CH/Ar demonstrate that the orbital angular momentum of the CH ground-state term is partially quenched. A model in which a low-symmetry crystal field reduces the angular momentum quantitatively accounts for the observed behavior. Least-squares fitting the zeroth-moment data yields an empirical spin−orbit (SO) coupling coefficient of $A_\Pi = 21 \pm 1$ cm^{-1} and an orbital reduction factor of $\kappa = 0.26 \pm 0.03$. These in turn give a crystal-field (CF) splitting parameter of $V_\Pi = 78 \pm 15$ cm^{-1} and a net SO−CF splitting of $\Delta_\Pi \approx 81$ cm^{-1} for the X $^2\Pi$ term of CH/Ar. The magnitude of the CF effect is comparable to that found for the ground-state term of OH/Ar.[1,13]

The double-signed MCD of the A $^2\Delta \leftarrow$ X $^2\Pi$ system and single-signed MCD of B $^2\Sigma^-$ and C $^2\Sigma^+ \leftarrow$ X $^2\Pi$ systems are readily explained by orbital reduction in the ground state, which substantially enhances the intensity of A terms in the former at the expense of the latter. The magnetic-field dependence of the first MCD moment of the A $^2\Delta \leftarrow$ X $^2\Pi$ system gives an empirical excited-state SO coupling coefficient of $A_\Delta = 5 \pm 1$ cm^{-1}, which must arise predominantly from external-atom effects involving interactions with Ar atoms of the host medium. The separation between extrema of the sigmoidal-shaped (A-term) feature of the A $^2\Delta$ MCD suggests an excited-state CF splitting of $V_\Delta \lesssim 15$ cm^{-1}, substantially smaller than the CF splitting of the ground state.

Acknowledgment. We thank Dr. Janna Rose for supplying us with earlier data for CH/Ar. This research was conducted with partial funding from the New Zealand Lottery Grant Board, Grant GR 2224987.

References and Notes

(1) Langford, V. S.; Williamson, B. E. *J. Phys. Chem. A* **1997**, *101*, 3119−3124.

(2) Herzberg, G. *Molecular Spectra and Molecular Structure Volume 1: Spectra of Diatomic Molecules*, 2nd ed.; Krieger: New York, 1950.

(3) Huber, K. P.; Herzberg, G. *Molecular Spectra and Molecular Structure, Volume 4: Constants of Diatomic Molecules*; Van Nostrand Reinhold: New York, 1979.

(4) Gaydon, A. G. *Spectroscopy and Combustion Theory*; Chapman and Hall Ltd: London, 1948.

(5) Smith, D. *Chem. Rev.* **1992**, *92*, 1473−1485.

(6) Wyckoff, S.; Telger, S.; Wehinger, P. A.; Spinrad, H.; Belton, M. J. *Astrophys. J.* **1988**, *325*, 927−938.

(7) Singh, M.; Chaturvedi, J. P. *J. P. Astrophys. Space Sci.* **1987**, *136*, 231−246.

(8) Ninkov, Z.; Walker, G. A. H.; Yang, S. *Astrophys. J.* **1987**, *321*, 425−437.

(9) Robinson, G. W.; McCarty, M. J. *J. Am. Chem. Soc.* **1960**, *82*, 1859−1864.

(10) Keyser, L. F. Ph.D. Dissertation, California Institute of Technology, Pasadena, 1965.

(11) Milligan, D. E.; Jacox, M. E. *J. Chem. Phys.* **1967**, *47*, 5146−5156.

(12) Rose, J. L. Ph.D. Dissertation, University of Virginia, Charlottesville, 1987.

(13) Langford, V. S. Ph.D. Dissertation, University of Canterbury, Christchurch, 1997.

(14) Piepho, S. B.; Schatz, P. N. *Group Theory in Spectroscopy with Applications to Magnetic Circular Dichroism*; Wiley-Interscience: New York, 1983.

(15) Dunford, C. L. Ph.D. Dissertation, University of Canterbury, Christchurch, 1997.

(16) Dunford, C. L.; Williamson, B. E. *J. Phys. Chem. A* **1997**, *101*, 2050−2054.

(17) Botterud, I.; Loftus, A.; Veseth, L. *Phys. Scr.* **1973**, *8*, 218−224.

(18) Williamson, B. E.; Roser, D. C.; Vala, M. *J. Phys. Chem.* **1994**, *98*, 3624−3630.

(19) Linevsky, M. J. *J. Chem. Phys.* **1967**, *47*, 3485−3490.

(20) Samet, C.; Rose, J. L.; Schatz, P. N.; O'Brien, M. C. M. *Chem. Phys. Lett.* **1989**, *159*, 567−572.

(21) Lund, P. A.; Smith, D.; Jacobs, S. M.; Schatz, P. N. *J. Phys. Chem.* **1984**, *88*, 31−42.